Chinese Chemical Letters 37 (2026) 111780

Contents lists available at ScienceDirect

Chinese Chemical Letters

journal homepage: www.elsevier.com/locate/cclet

Anti-MRSA anthrone–macrolide hybrids from the ascomycete fungus *Neonectria* sp.

Jinwei Ren[a,1], Ruiyun Huo[a,1], Xiaoqi Sun[a,1], Guobo Guan[a], Ying Shi[a], Yangyang Han[c], Yongsheng Che[c,*], Ling Liu[a,b,*]

[a] State Key Laboratory of Microbial Diversity and Innovative Utilization, Institute of Microbiology, Chinese Academy of Sciences, Beijing 100101, China
[b] College of Life Sciences, University of Chinese Academy of Sciences, Beijing 100049, China
[c] State Key Laboratory of Bioactive Substance and Function of Natural Medicines, Institute of Medicinal Biotechnology, Chinese Academy of Medical Sciences & Peking Union Medical College, Beijing 100050, China

ARTICLE INFO

Article history:
Received 2 June 2025
Revised 15 August 2025
Accepted 1 September 2025
Available online 2 September 2025

Keywords:
Ascomycete fungus
Heterodimer
Structure elucidation
Chemical calculations
Anti-MRSA activity

ABSTRACT

Two novel anthrone–macrolide hybrids, neonectones A and B (**1** and **2**), one new 10-membered macrolide neonectone C (**3**), and one new oxaphenalenone derivative, (±)-neonectone D (**4**), together with five known compounds (**5**–**9**) were isolated from the crude extract of the ascomycete fungus *Neonectria* sp. Compounds **1** and **2** represent the first example of anthrone–ten-membered lactone heterodimers, possessing an unprecedented 5-(10-oxo-9,10-dihydroanthracen-9-yl)oxecane-2,7–dione skeleton. Their structures and absolute configurations were established by a combination of extensive spectroscopic analysis, ^{13}C nuclear magnetic resonance spectroscopy (NMR) chemical shifts calculations with DP4+ probability analysis and electronic circular dichroism (ECD) calculations. Bioactivity evaluation revealed that compounds **1**, **2** and **9** exhibited anti-methicillin-resistant *Staphylococcus aureus* (MRSA) activity. Compound **9** exhibited anti-MRSA activity through disrupting membrane integrity, suppressing energy and nucleotide metabolism, modulating membrane transport and transcription/translation regulatory factors, as well as inhibiting quorum sensing and biofilm formation.

© 2026 Published by Elsevier B.V. on behalf of Chinese Chemical Society and Institute of Materia Medica, Chinese Academy of Medical Sciences.

Natural products have been crucial in drug discovery and development processes, owing to their unique and varied chemical structures and a wide range of biological activities [1–3]. Ten-membered lactones (TMLs), a large group of natural polyketides, are characterized by a macrolide lactone core substituted with various alkyl, aryl, and oxygen groups depending on their natural sources, such as fungi, bacteria, marine organisms, and insects [4]. These compounds display diverse biological activities, including cytotoxic, phytotoxic, antimalarial, antifungal, antibacterial and enzyme inhibitory effects, making them an interesting and diverse group for research [4–6].

The genus *Neonectria* has been proven to produce a variety of bioactive secondary metabolites including terpenes, alkaloids, polyketides, *etc.* [7–10]. Many of these possess promising biological activities, such as cytotoxic, antimalarial and antimicrobial activities. During our ongoing efforts to search for new bioactive metabolites from fungi in unique environments [11–13], *Neonectria* sp. RXZ010, a fungus was isolated from a soil sample collected from the Qinghai-Tibetan plateau, Chayu, People's Republic of China. Previous chemical investigations of *Neonectria* sp. RXZ010 led to the isolation of neonectrolides A–E, and their putative precursors [7,8]. In order to enrich and improve the chemical space of *Neonectria* sp. RXZ010, we carried out a further chemical study on this fungus. Careful chemical investigations on the remaining fractions led to the isolation and characterization of two novel anthrone–macrolide hybrids, neonectones A and B (**1** and **2**), one new 10-membered macrolide neonectone C (**3**), and one new oxaphenalenone analogue (±)-neonectone D (**4**), together with five known compounds (**5**–**9**) (Fig. 1) [7,14–16]. To the best of our knowledge, compounds **1** and **2** represent the first example of anthrone–ten-membered macrolide hybrids, possessing an unprecedented 5-(10-oxo-9,10-dihydroanthracen-9-yl)oxecane-2,7–dione skeleton. All the isolated compounds were evaluated for their anti-methicillin-resistant *Staphylococcus aureus* (MRSA) activity. Among them, compounds **1**, **2** and **9** exhibited notable anti-MRSA effects. Furthermore, the *in vivo* activity of compound **9** was assessed using a *Galleria mellonella* infection model, and its an-

* Corresponding authors.
E-mail addresses: ysche@imb.cams.cn (Y. Che), liul@im.ac.cn (L. Liu).
[1] These authors contributed equally to this work.

https://doi.org/10.1016/j.cclet.2025.111780
1001-8417/© 2026 Published by Elsevier B.V. on behalf of Chinese Chemical Society and Institute of Materia Medica, Chinese Academy of Medical Sciences.

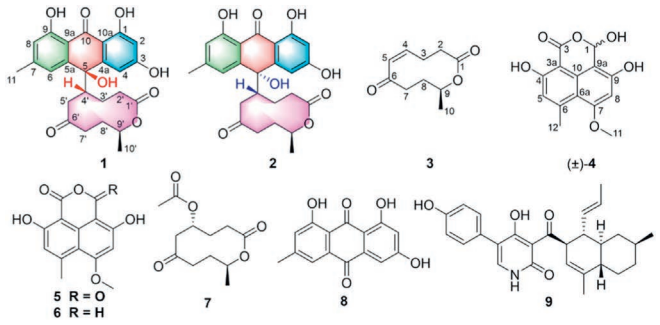


Fig. 1. Chemical structures of compounds **1**–**9**.

tibacterial mechanism was also investigated. The isolation, structure elucidation, and biological activities of these compounds are detailed in this paper.

Neonectone A (**1**) was obtained as pale yellow solid and its molecular formula was established as $C_{25}H_{26}O_8$ based on the (high resolution electrospray ionization mass spectrometry) HRESIMS data at *m/z* 477.1520 $[M+Na]^+$ (calcd. for $C_{25}H_{26}O_8Na$, 477.1518), indicating 13 degrees of unsaturation. Detailed interpretation of the 1D nuclear magnetic resonance spectroscopy (NMR) and heteronuclear singler quantum correlation (HSQC) data (Table S1 in Supporting information) of **1** revealed the presence of 25 carbon resonances corresponding to two methyls, five sp^3 methylenes, two sp^3 methines with one oxygenated, one oxygenated tertiary carbon (δ_C 73.8), twelve aromatic carbons, one ester carbonyl carbon (δ_C 172.6) and two carbonyl carbons (δ_C 209.5 and 189.5, respectively). These data accounted for all ^1H and ^{13}C NMR resonances of **1** except for one unobserved exchangeable proton, suggesting that **1** was a tetracyclic compound. The heteronuclear multiple bond correlation (HMBC) correlations (Fig. S1 in Supporting information) from H-2 to C-1, C-3, C-4 and C-10a, from H-4 to C-3, C-4a, C-5, C-10a and C-10, from H-6 to C-5, C-7, C-8, C-9a and C-10, from H-8 to C-6, C-9 and C-9a permitted the completion of the anthracen-9(10*H*)-one moiety (Unit A). The hydroxyl groups were located at C-1, C-3 and C-9, respectively, which was deduced by the HMBC correlations from OH-1 to C-1, C-2 and C-10a, and from OH-9 to C-8, C-9 and C-9a, as well as the chemical shift of C-3 (δ_C 165.4). Meanwhile, the HMBC correlations from H_3–11 to C-6, C-7 and C-8 indicated that the methyl carbon C-11 was located at the C-7. In addition, the ^1H–^1H correlation spectroscopy (COSY) (Fig. S1) correlations of H_2–2′/H_2–3′/H-4′/H_2–5′, and of H_2–7′/H_2–8′/H-9′/H_3–10′, as well as the HMBC correlations from H_2–2′ and H-9′ to C-1′, and from H_2–5′ and H_2–7′ to C-6′ suggested the presence of 10-methyloxecane-2,7–dione unit (Unit B). Moreover, the HMBC correlations from H_2–5′ to C-5, and from OH-5 to C-5 and C-4′ permitted the connection of units A and B *via* a C-5–C-4′ linkage with the hydroxyl group OH-5 located at C-5. Thus, the planar structure of **1** was established as shown (Fig. 1).

The absolute configuration of C-9′ in **1** was deduced as 9′*S* on the basis of biosynthetic consideration and by analogy to the co-isolated putative precursor **7** [7]. However, the relative configurations of C-5 and C-4′ in **1** could not be assigned due to the lack of relevant rotating frame overhauser effect spectroscopy (ROESY) correlations. Due to the presence of the remaining two stereogenic centers (C-5 and C-4′), one of the four stereoisomers (5*R*,4′*R*,9′*S*)-(**1a**), (5*R*,4′*S*,9′*S*)-(**1b**), (5*S*,4′*R*,9′*S*)-(**1c**) and (5*S*,4′*S*,9′*S*)-(**1d**) must represent the actual configuration of **1**. Then the gauge-including atomic orbital (GIAO) ^{13}C NMR calculations of four stereoisomers **1a**–**1d** were employed at the mPW1PW91/6 + 31G(d) level. The experimental NMR data of **1** was compared with those calculated of **1a**–**1d** using the linear correlation coefficients (R^2) obtained by linear regression analysis, root-mean-square error (RMSE) and DP4+ probability analysis [17,18]. The calculated chemical shifts for **1a** and **1c** matched well with the experimental values of **1** with high correlation coefficients (R^2) and small RMSE in carbon data analysis (Fig. 2). In addition, the experimental and calculated chemical shifts were further statistically analyzed by DP4+ probability. The results showed (5*R*,4′*R*,9′*S*)-(**1a**) and (5*S*,4′*R*,9′*S*)-(**1c**) may be the most suitable structure for **1**, which had a high probability of 48.9 % and 51.1 % (Fig. 2), respectively. Thus, the above data indicated that the (5*R*,4′*R*,9′*S*)-(**1a**) and (5*S*,4′*R*,9′*S*)-(**1c**) may be the correct relative structures for **1**. In order to establish the absolute configuration of **1**, the electronic circular dichroism (ECD) spectra of (5*R*,4′*R*,9′*S*)-(**1a**) and (5*S*,4′*R*,9′*S*)-(**1c**) were further calculated. As a result, the experimental ECD spectrum of **1** matched well with the calculated ECD curve of (5*R*,4′*R*,9′*S*)-(**1a**) (Fig. S2 in Supporting information), suggesting the 5*R*,4′*R*,9′*S* absolute configuration.

Neonectone B (**2**) was also obtained as pale yellow solid and was assigned the same molecular formula $C_{25}H_{26}O_8$ (13 degrees of unsaturation) as **1** by HRESIMS (*m/z* 477.1523 $[M+Na]^+$) and NMR data (Table S1). Comparison of the 1D NMR data (Table S1) and 2D NMR data (Fig. S1) of **2** with those of **1** revealed the same structural features as those of **1**, suggesting their diastereomeric relationship. The absolute configuration of C-9′ in **2** was also deduced as 9′*S* on the basis of biosynthetic consideration [7]. To assign the relative configurations of C-5 and C-4′ in **2**, the calculated chemi-

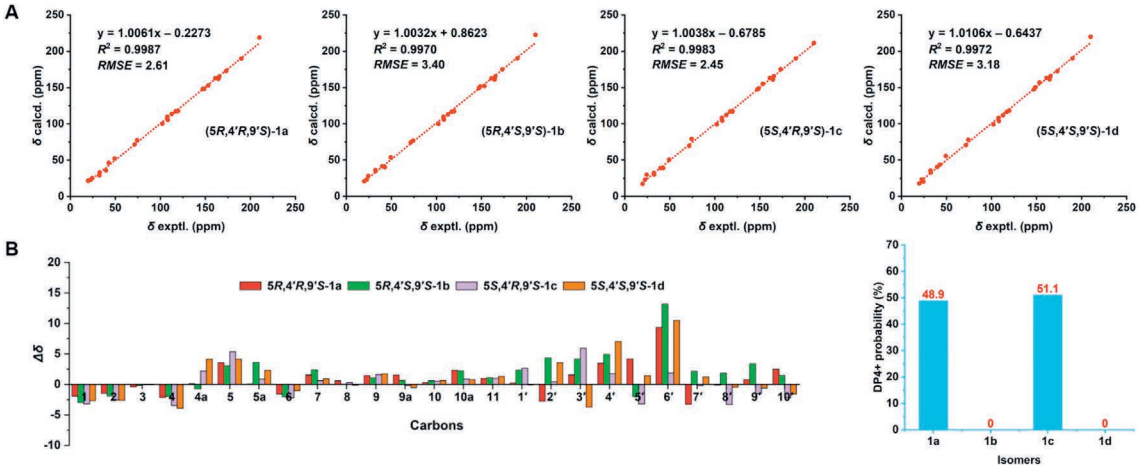


Fig. 2. The ^{13}C NMR calculation results of two plausible isomers of **1**. (A) Linear correlation plots of calculated *vs.* experimental ^{13}C NMR chemical shifts. (B) Relative errors between the calculated ^{13}C NMR chemical shifts the recorded data and DP4+ probability analysis.

cal shifts of **1a**–**1d** were further compared with the experimental data of **2** using linear correlation, RMSE, and the DP4+ probability analysis. High R^2 values of 0.9980 for **1a** and 0.9981 for **1c** were obtained (Fig. S3 in Supporting information), indicating that the calculated δ_C of **1a** and **1c** matched the experimental δ_C very well. Moreover, according to the DP4+ probability analyses, **1a**, **1b**, **1c** and **1d** were assigned with 52.5 %, 0 %, 47.5 % and 0 %, respectively. Eventually, the relative configuration of **2** could be determined to be either(5*R*,4′*R*,9′*S*)-(**1a**) and (5*S*,4′*R*,9′*S*)-(**1c**). To further define its absolute configuration, the calculated ECD spectra of (5*R*,4′*R*,9′*S*)-(**1a**) and (5*S*,4′*R*,9′*S*)-(**1c**) were compared with the experimental ECD curve of **2**. As shown in Fig. S2, the experimental ECD spectrum of **2** was nearly identical to the calculated ECD spectrum of (5*S*,4′*R*,9′*S*)-(**1c**), which determined the absolute configuration of **2** as 5*S*,4′*R*,9′*S*.

Neonectone C (**3**) was obtained as a white powder. Its molecular formula, $C_{10}H_{14}O_3$, with four degrees of unsaturation, was established based on the HRESIMS data at *m/z* 205.0840 $[M+Na]^+$ (calcd. for $C_{10}H_{14}O_3Na$, 205.0835). The 1D NMR and HSQC spectra exhibited 10 carbon signals corresponding to one methyl carbon, four methylene carbons, one oxygenated carbon, two olefinic carbons, one ester carbonyl carbon (δ_C 170.9) and one carbonyl carbon (δ_C 205.4). Analysis of the ^1H–^1H COSY NMR data (Fig. S1) led to the identification of the two isolated proton spin-systems of C-2–C-3–C-4–C-5 and C-7–C-8–C-9–C-10. The HMBC correlations (Fig. S1) from H-4 and H-5 to C-6 (δ_C 205.4), and from H_2–7 to C-5 and C-6 indicated that C-6 was attached to both C-5 and C-7. Furthermore, HMBC correlations from H_2–2 and H_2–3 to C-1 and from H-9 to C-1 established the C-1–C-2 linkage and the ether linkage between C-1 and C-9, thereby completing the planar structure of **3**. The absolute configuration of C-9 in **3** was also deduced as 9*S* based on biogenetic comparison with the co-isolated 3-dehydroxy-4-*O*-acetylcephalosporolide C (**7**) [13]. Thus, the structure of **3** was established as shown (Fig. 1).

Neonectone D (**4**) was obtained as a yellow powder, and its molecular formula was deduced to be $C_{14}H_{12}O_6$, based on the HRESIMS data at *m/z* 277.0706 $[M+H]^+$ (calcd. for $C_{14}H_{13}O_6$, 277.0707), implying nine degrees of unsaturation. Its NMR data (Table S2 in Supporting information) exhibited a great similarity to those of lamellicolic anhydride (**5**), except that the carbonyl carbon at the C-1 position in **5** was reduced to a hydroxy moiety in **3**. This was evidenced by the HRESIMS data, the chemical shift of C-1 (δ_C 94.2) and the HMBC correlations (Fig. S1) from H-1 to C-3, C-9, C-9a and C-10. The small specific rotation value revealed that **4** was a racemate, due to the existence of a hemiacetal at C-1. However, chiral-phase resolution using different conditions failed. Therefore, the structure of **4** was established as neonectone D, as depicted.

In addition, the known compounds were elucidated as lamellicolic anhydride (**5**) [14], corymbiferan lactone E (**6**) [7], 3-dehydroxy-4-*O*-acetylcephalosporolide C (**7**) [7], emodin (**8**) [15], and ilicicolin H (**9**) [16], by comparing their NMR data with the reported literature values.

Neonectones A and B (**1** and **2**) represent the first example of the anthrone–macrolide hybrids possessing an unprecedented 5-(10-oxo-9,10-dihydroanthracen-9-yl)oxecane-2,7–dione skeleton. Up to now, the reported carbon skeleton of anthrone heterodimers mainly include anthrone–cyclohexene [19,20], anthrone–pyrano [21], anthrone–anthraquinone [22] and anthrone *C*-glycosides [23]. The anthrone–macrolide hybrids such as **1** and **2** have never been reported. Compound **3** is a new analogue of compound **7**. While compound **4** was isolated as a racemate. The putative biosynthetic pathways of these compounds were also proposed in Scheme S1 (Supporting information).

Compounds **1**–**9** were screened for their antibacterial activities against MRSA. Compounds **1**, **2** and **9** exhibited anti-MRSA activity with minimum inhibitory concentration (MIC) values of 16, 32 and 8 μg/mL, respectively (Table S5 in Supporting information), while the MIC value of the positive control vancomycin (Van) was 2 μg/mL. To evaluate the potential synergistic effects, these three compounds were combined with Van using the checkerboard method. The MIC of compound **9** decreased to 4 μg/mL when combined with Van, while the MIC of Van was reduced to 1 μg/mL in the combination of all three compounds. The fractional inhibitory concentration index (FICI) value of the combination of compound **9** and Van was 1, indicating an additive effect against MRSA. These results suggested that compound **9** can enhance the antibacterial effect of Van, highlighting its potential as an adjunctive therapeutic agent. In contrast, compounds **1** and **2** exhibited FICI values of 1.5 when combined with Van, indicating neither synergistic nor additive antibacterial activity. Due to limited quantities, the antibacterial mechanisms of compounds **1** and **2** were not investigated. Compound **9** has been previously identified as a broad-spectrum antifungal agent targeting *Cryptococcus*, *Candida* and *Aspergillus* species by inhibiting mitochondrial cytochrome bc_1 reductase [24]. It also exhibits anticancer activity against colon adenocarcinoma, non-small cell lung cancer, prostate cancer, and hepatocellular carcinoma [25]. In the present study, compound **9** demonstrated significant anti-MRSA activity, with its antibacterial mechanism yet to be elucidated.

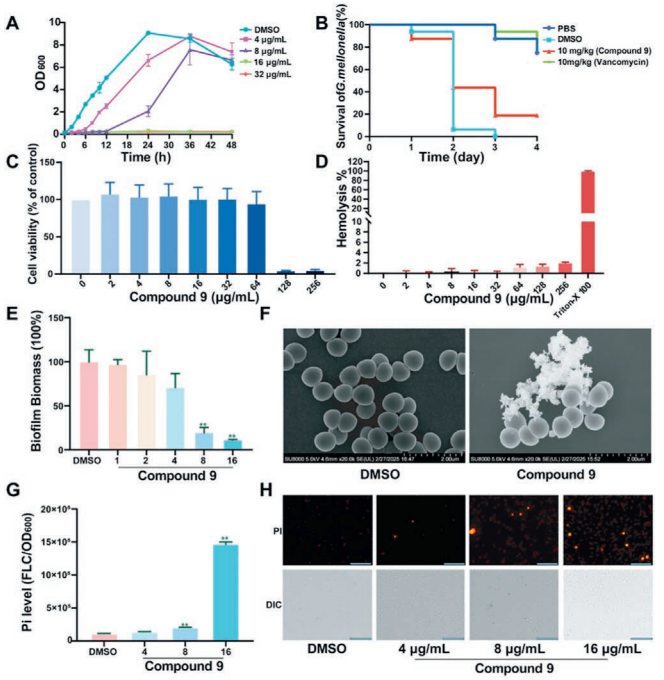


Fig. 3. Anti-MRSA activity and safety evaluation of compound **9**. (A) Growth inhibition of MRSA by compound **9**. (B) Antimicrobial activity of compound **9** in a MRSA-infected *G. mellonella* model. (C) Cytotoxicity of compound **9** against RAW264.7 cell lines. (D) Hemolytic test for compound **9**. (E) The effect of compound **9** on MRSA biofilm formation. (F) SEM images of MRSA after treatment with DMSO (control) and compound **9**, respectively. Scale bar: 2 μm. (G, H) The PI fluorescence intensity was measured in DMSO and compound **9**-treated groups. Scale bar: 10 μm. Data are expressed as mean ± standard deviation (SD) ($n = 3$). $^{**}P < 0.01$ *vs.* the DMSO group.

To further verify the anti-MRSA activity of compound **9**, bacterial growth curves were measured at various concentrations of **9**. As shown in Fig. 3A, sub-MIC (4 μg/mL, 1/2× MIC) and MIC concentrations (8 μg/mL) of compound **9** inhibited MRSA growth, while higher concentrations (16 μg/mL, 2× MIC; 32 μg/mL, 4× MIC) exhibited rapid bactericidal activity. To validate these *in vitro* results, a *G. mellonella* infection model was used, which is suitable for antimicrobial evaluation due to its similar innate immune sys-

tem to mammals [26]. Survival analysis revealed that compound **9** significantly improved the survival rate of *G. mellonella* compared to the DMSO control group (18.7 % survival rate at 4 day, Fig. 3B), indicating its *in vivo* anti-MRSA efficacy. Additionally, compound **9** exhibited no obvious toxicity against macrophages (RAW264.7) across a broad concentration range (0–64 μg/mL, Fig. 3C). In the hemolysis assays, compound **9** exhibited minimal hemolytic activity (<5 % hemolysis rate) even at 256 μg/mL (32× MIC, Fig. 3D).

MRSA is a classic biofilm-forming pathogen responsible for a variety of chronic infections [27]. To evaluate the anti-biofilm potential of compound **9**, its effect on MRSA biofilm formation were tested at five concentrations (ranging from 1/8× MIC to 2× MIC). Results showed that concentrations of the MIC and 2× MIC of compoud **9** significantly inhibited MRSA biofilm formation (Fig. 3E), indicating a dose-dependent inhibitory effect. Scanning electron microscopy (SEM) analysis revealed treatment with compound **9** at the MIC concentration caused bacterial cell wall and membrane rupture, with complete collapse within 8 h (Fig. 3F). This suggested that compound **9** disrupted MRSA cell membrane integrity, a critical factor in its antibacterial activity. Consistent with these findings, cell membrane permeability assays demonstrated that compound **9** increased the number of PI (propidium iodide)-positive cells (dead cells stained red) in a concentration-dependent manner (Figs. 3G and H).

To further elucidate the antibacterial mechanism of compound **9** against MRSA, transcriptomic analysis was conducted after treatment at the MIC concentration. Compared to the DMSO control group, the compound **9**-treated group exhibited 1011 differentially expressed genes (DEGs), including 514 upregulated and 497 downregulated genes (Fig. 4A). Gene ontology (GO) functional enrichment analysis of these DEGs revealed significant enrichment in pathways associated with transmembrane transport, ATP-dependent energy metabolism, oxidative phosphorylation, purine and pyrimidine nucleotide metabolism, as well as glucose metabolism (Fig. 4B). RNA sequencing and quantitative reversed transcription polymerase chain reaction (qRT-PCR) validation showed that compound **9** significantly downregulated the expression of genes involved in ATP-dependent activity (*RS13605*, *RS05255*, *RS05260* and *mnhD2*) (Fig. 4C). Given the role of quorum sensing (QS) in bacterial pathogenicity [28], we examined QS-related genes and found that compound **9** downregulated the expression of *RS01060*, *RS01055* and *RS01065* (Fig. 4D). Futhermore, considering the important involvement of membrane transport, transcription and translation regulatory factors in MRSA resistance mechanisms [29,30], RNA sequencing and qRT-PCR results further indicated that compound **9** modulated the expression of genes encoding translation and transcription factors (Figs. 4E and F) and regulated the expression of membrane transport-related genes (Fig. 4G). Additionally, compound **9** also regulated the expression of genes related to nucleotide metabolism in MRSA (Fig. 4H).

In conclusion, neonectones A and B (**1** and **2**), two unprecedented anthrone–macrolide hybrids, along with their possible biosynthetic precursors were isolated from the fungus *Neonectria* sp. To the best of our knowledge, this is the first time to report the anthrone–macrolide hybrid natural products. Biogenetically, these novel hybrids **1** and **2** could be derived from the co-isolated neonectone C (**3**) and emodin (**8**) *via* a Michael addition. Compounds **1**, **2** and **9** exhibited antibacterial activity against MRSA. Compound **9** exerted its anti-MRSA activity though disrupting membrane integrity, suppressing energy and nucleotide metabolism, modulating membrane transport and transcription/translation regulatory factors, as well as inhibiting QS and biofilm formation (Fig. 4I). These findings not only expand the structural diversity of anthrone heterodimers, but also provide promising antibacterial candidates for combating resistant bacterial pathogen MRSA.

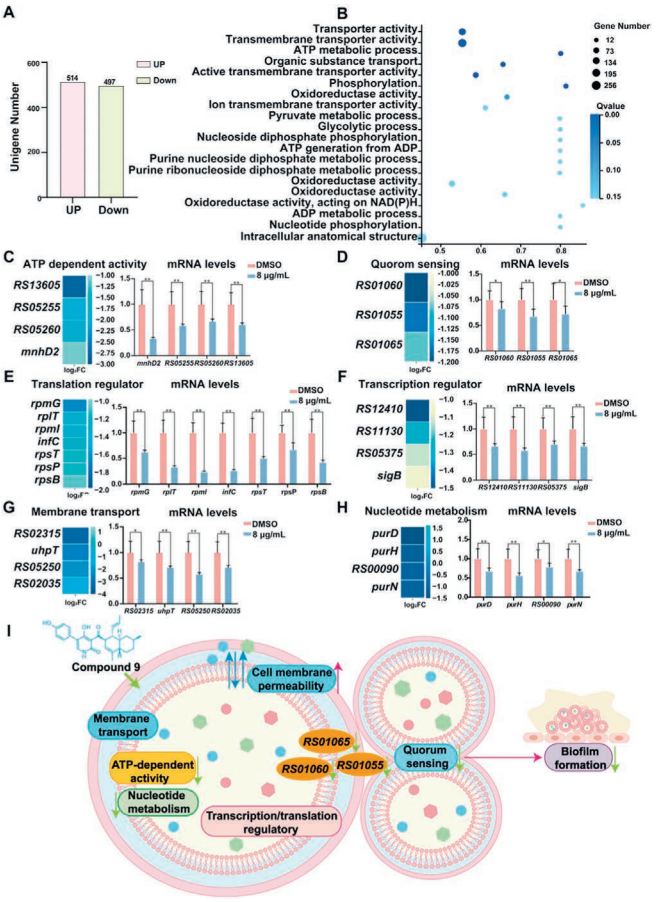


Fig. 4. Transcriptomic analysis revealed antibacterial mechanism of compound **9**. (A) Differential gene expression between DMSO control and compound **9**-treated MRSA revealed by RNA-seq analysis (514 genes up-regulated and 497 genes down-regulated). (B) Top 20 pathways enriched in compound **9**-treated MRSA compared to the DMSO group, determined through GO analysis. The Y-axis represents GO functional classification, the X-axis represents the Q-value, and the dots represent the number of genes annotated with GO entries. (C–H) Selected gene clustering following RNA-seq analysis, with DEGs expression levels verified by qRT-PCR. Data are presented as mean ± SD ($n = 3$). $^{*}P < 0.05$, $^{**}P < 0.01$ *vs.* the DMSO group. (I) Proposed mechanistic model of compound **9**'s anti-MRSA activity.

Declaration of competing interest

The authors declare that they have no known competing financial interests or personal relationships that could have appeared to influence the work reported in this paper.

CRediT authorship contribution statement

Jinwei Ren: Methodology, Investigation, Formal analysis, Data curation. **Ruiyun Huo:** Writing – original draft, Validation, Software, Methodology, Investigation, Formal analysis, Data curation. **Xiaoqi Sun:** Writing – original draft, Visualization, Validation, Software, Methodology, Investigation, Data curation. **Guobo Guan:** Methodology, Investigation, Data curation. **Ying Shi:** Visualization, Software, Methodology, Investigation. **Yangyang Han:** Software, Methodology. **Yongsheng Che:** Writing – review & editing, Writing – original draft, Visualization, Validation, Supervision, Resources, Project administration, Investigation, Formal analysis, Data curation, Conceptualization. **Ling Liu:** Writing – review & editing, Writing – original draft, Visualization, Validation, Supervision, Software, Resources, Project administration, Methodology, Investigation, Funding acquisition, Formal analysis, Data curation, Conceptualization.

Acknowledgments

This research was funded by grants from the National Key Research and Development Program of China (No. 2022YFC2303100) and the National Natural Science Foundation of China (Nos. 32472320, 32022002).

Supplementary materials

Supplementary material associated with this article can be found, in the online version, at doi:10.1016/j.cclet.2025.111780.

References

[1] D.J. Newman, G.M. Cragg, J. Nat. Prod. 83 (2020) 770–803.
[2] Z.W. Luo, F.C. Yin, X.B. Wang, et al., Chin. J. Nat. Med. 22 (2024) 195–211.
[3] Y. Shi, M.H. Ji, J.Y. Dong, et al., Mycology 15 (2024) 283–321.
[4] G. Dräger, A. Kirschning, R. Thiericke, et al., Nat. Prod. Rep. 13 (1996) 365–375.
[5] P. Sun, S. Lu, T.V. Ree, et al., Curr. Med. Chem. 19 (2012) 3417–3455.
[6] V. Dubovik, A. Dalinova, A. Berestetskiy, Nat. Prod. Rep. 41 (2024) 85–112.
[7] J.W. Ren, F. Zhang, X.Y. Liu, et al., Org. Lett. 14 (2012) 6226–6229.
[8] J.W. Ren, S.B. Niu, L. Liu, et al., J. Nat. Prod. 78 (2015) 1316–1321.
[9] Y. Shiono, K. Shimanuki, F. Hiramatsu, et al., Bioorg. Med. Chem. Lett. 18 (2008) 6050–6053.
[10] C. Nirma, V. Eparvier, D. Stien, J. Nat. Prod. 78 (2015) 159–162.
[11] L. Liu, Y. Li, S. Liu, et al., Org. Lett. 11 (2009) 2836–2839.
[12] L. Liu, X. Chen, D. Li, et al., J. Nat. Prod. 78 (2015) 746–753.
[13] J.Y. Zhang, Y. Li, F.X. Ren, et al., J. Nat. Prod. 82 (2019) 1678–1685.
[14] N.J. McCorkindale, A. McRitchie, S.A. Hutchinson, J. Chem. Soc. Chem. Commun. (1973) 108–109.
[15] Y.C. Yang, M.Y. Lim, H.S. Lee, J. Agric. Food Chem. 51 (2003) 7629–7631.
[16] Z. Zhang, C.S. Jamieson, Y.L. Zhao, et al., J. Am. Chem. Soc. 141 (2019) 5659–5663.
[17] X. Zhang, J. Li, K.Z. Lu, et al., Chin. Chem. Lett. 35 (2024) 109456.
[18] X.Y. Hu, X.M. Li, S.Q. Yang, et al., Chin. Chem. Lett. 34 (2023) 107516.
[19] W.M. Zhong, J.F. Wang, X.Y. Wei, et al., Org. Lett. 20 (2018) 4593–4596.
[20] W.M. Zhong, J.F. Wang, X.Y. Wei, et al., Tetrahedron Lett. 60 (2019) 1600–1603.
[21] G.D. Chen, Y.R. Bao, Y.F. Huang, et al., Fitoterapia 92 (2014) 252–259.
[22] A.R. Carroll, B.D. Nash, S. Duffy, et al., J. Nat. Prod. 75 (2012) 1206–1209.
[23] Y. Koyama, R. Yamaguchi, K. Suzuki, Angew. Chem. Int. Ed. 47 (2008) 1084–1087.
[24] S.B. Singh, W. Liu, X. Li, et al., Bioorg. Med. Chem. Lett. 23 (2013) 3018–3022.
[25] E.A. Guzmán, T.P. Pitts, K.R. Tandberg, et al., Mar. Drugs 19 (2021) 73.
[26] H. Lu, Y. Tan, Y. Zhang, et al., Fitoterapia 159 (2022) 105201.
[27] G. Yu, T.Y. Huang, Y. Li, Microb. Pathog. 196 (2024) 106986.
[28] Y.S. Wang, Z.R. Bian, Y. Wang, Appl. Microbiol. Biotechnol. 106 (2022) 6365–6381.
[29] H.F. Chambers, F.R. DeLeo, Nat. Rev. Microbiol. 7 (2009) 629–641.
[30] D.N. Brawley, D.B. Sauer, J.P. Li, et al., Nat. Chem. Biol. 18 (2022) 706–712.